Endovaginal Ultrasonography: Methodology and Normal Pelvic Floor Anatomy

6

Giulio Aniello Santoro, Andrzej Paweł Wieczorek, S. Abbas Shobeiri and Aleksandra Stankiewicz

Abstract High-resolution three-dimensional endovaginal ultrasonography (EVUS) provides a detailed evaluation of the pelvic floor muscles and the levator ani complex, the lower urinary tract, and the anorectal region in planes that cannot be determined by conventional two-dimensional EVUS. Multiplanar reconstruction and rendering techniques allow the investigator to correctly recognize and measure specific anatomic elements of the pelvic floor and to understand their true spatial relationships (anterior, lateral, and posterior compartments). This modality is relatively easy to perform and is time efficient, correlates well with other imaging modalities, and delivers relevant information in patients with pelvic floor disorders.

Keywords Anal sphincters • Endovaginal ultrasonography • Levator ani • Levator hiatus • Pelvic floor • Perineal muscles • Pubovisceral muscle • Three-dimensional ultrasonography • Urethral complex • Urogenital hiatus

6.1 Introduction

Endovaginal ultrasonography (EVUS) has become a valuable tool in the diagnostic workup of patients with pelvic floor disorders, and it provides sufficient information for clinical decision making in many cases [1, 2]. However, with the conventional two-dimensional (2D) ultrasound (US), there are many elements of the image that cannot be correctly recognized as components of a three-dimensional (3D) structure, or at least not perceived in their true spatial relationships, and a good deal of relevant information may remain hidden.

As the transition towards total digital image acquisition continues, 3D ultrasound, constructed from a synthesis of a high number of parallel transaxial 2D images, has been developed [3]. After a 3D dataset has been acquired, it is immediately possible to select coronal anterior–posterior or posterior–anterior as well as sagittal right–left views, together with any oblique image plane. Three-dimensional US, particularly developed for obstetric applications during the last 15 years, has been shown to be a useful adjunct to conventional 2D-US for evaluation of the lower urinary tract, the levator ani complex, pelvic organ prolapse (POP), and anal sphincter imaging [4–7].

In this chapter we will review the methodology of 3D-EVUS (equipment, patient preparation, and patient position, technique of examination, manner of performing measurements) and evaluate the anatomy of the female pelvic floor (anterior, lateral, and posterior compartments) with this technique, providing a standardization both with regard to which levels of the pelvic floor and on which scan planes key anatomic structures can be described and measured.

G.A. Santoro
Pelvic Floor Unit and Colorectal Service, 1st Department of General Surgery, Regional Hospital, Treviso, Italy

G.A. Santoro, A.P. Wieczorek, C.I. Bartram (eds.) *Pelvic Floor Disorders*

6.2 Technical Aspects of 3D Endovaginal Ultrasound

We currently use the UltraView B-K Medical scanner (B-K Medical A/S, Mileparken 34, DK-2730 Herlev, Denmark) (Fig. 6.1). In order to obtain meaningful ultrasonic images, the operator must have an overall understanding of the technique and know how to use the controls available on the ultrasound device correctly. It is important to be aware that inadequate regulation of the equipment produces poor images and can lead to false-positive or false-negative diagnosis. Many types of ultrasound transducers have been developed for endovaginal assessment of the pelvic floor. The types of endoluminal probes include mechanical radial probes with a full 360° field, electronic biplanar probes with linear and transverse curved arrays, and endfire probes. The rotational transducer (type 2050, B-K Medical, Herlev, Denmark) has a shaft length of 270 mm, with a double crystal rotating at its tip. This probe has a frequency range from 6 to 16 MHz, with a focal length of 2–5 cm and a 90° scanning plane; it is rotated at 4–6 cycles/s, to give a radial scan of the surrounding structures (Figs. 6.2, 6.3).

The 2050 transducer has a built-in 3D automatic motorized system (the proximal–distal actuation mechanism and the electronic mover are fully enclosed within the housing of the probe) that allows acquisition of 300 transaxial images over a distance of 60 mm in 60 s, at the touch of a button, without requiring any movement relative to the investigated tissue (Fig. 6.4). The data from a series of closely spaced 2D images are combined to create a 3D volume displayed as a cube (Fig. 6.5) [3]. With the conventional 2D-US, the screen resolution is measured in number of pixels (display matrix: 700 × 700 pixel elements), with each pixel having a value between 0 and 255 (256 levels of grey). The result seen on the ultrasound monitor is a 2D image (X and Y plane only) with no depth information. Adding the third dimension means that the pixel is transformed in a small 3D picture element called a voxel, which will also have an assigned value

Fig. 6.1 The UltraView B-K Medical scanner

Fig. 6.2 The rotational transducer type 2050 (B-K Medical)

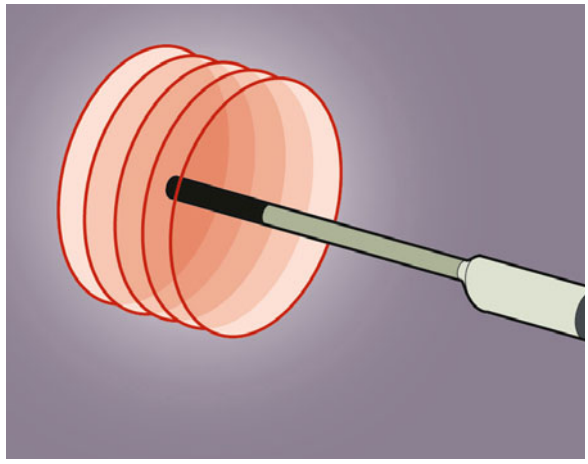

Fig. 6.3 The 2050 transducer is a mechanical radial probe with a full 360° field. It is rotated at 4–6 cycles per second and has a 90° scanning plane

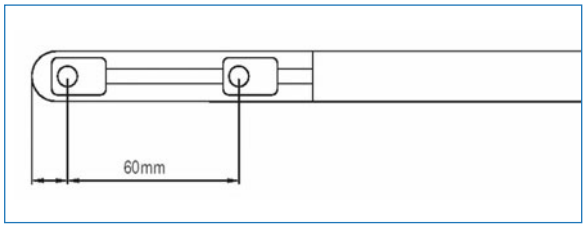

Fig. 6.4 The 2050 transducer has a built-in 3D automatic motorized system. The proximal–distal actuation mechanism and the electronic mover are fully enclosed within the housing of the probe; therefore, the 3D acquisition does not require any movement relative to the investigated tissue

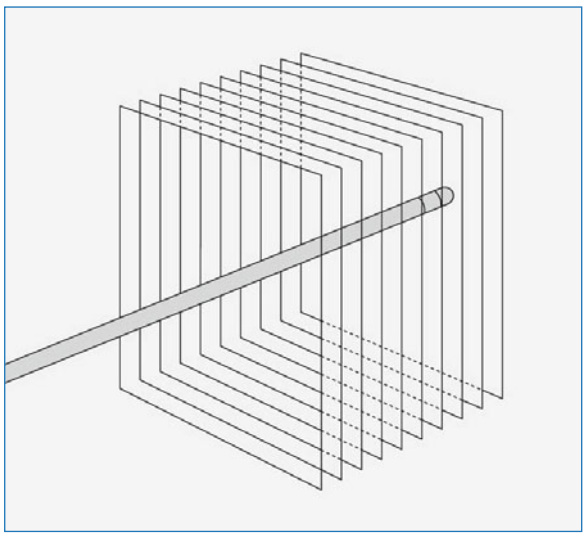

Fig. 6.5 A 3D volume, displayed as a cube, is created from a series of closely spaced 2D images (300 transaxial images over a distance of 60 mm)

between 0 and 255. Ideally, a voxel should be a cubic structure; however, the dimension in the Z plane is often slightly larger than that in the X and Y planes. The depth of the voxel is critical to the resolution of the 3D image, and this depth is directly related to the spacing between two adjacent images [3]. As already stated, the voxel should ideally form an exact cube, however sampling in the Z plane generally has slightly lower resolution than in the 700 × 700 matrix, due to acquisition speed. High-resolution 3D-US acquires four to five transaxial images sampled per millimeter of acquisition length in the Z plane. This means that an acquisition based upon sampling of transaxial images over a distance of 60 mm in the human body will result in a data volume block consisting of between 240 and 300 transaxial images. High-resolution data volumes will consist of typical voxel sizes around 0.15 × 0.15 × 0.2 mm. Because of this resolution in the longitudinal plane, which is close to the axial and transverse resolution of the 2D image, this technique ensures the true dimensions of the 3D data cube are also present in the reconstructed Z plane and provides accurate distance, area, angle, and volume measurements [8].

The ability to visualize information in the 3D image depends critically on the rendering technique [7]. Three basic types of technique are used.

1. *Surface render mode (SRM):* an operator or algorithm identifies the boundaries of the structures to create a wire-frame representation. It is the most commonly known version of render mode and is extensively used by some medical centers in producing perhaps the very first images of an unborn baby's facial contours. Surface rendering techniques only give good results when a surface is available to render, such as is possible for the puboviseral muscle assessed by 3D transperineal US (see Chapter 7) [9]. This technique, however, fails when a strong surface cannot be found such as in the subtly layered structures within the pelvic floor. SRM is, by its requirements, mainly a superficial postprocessed topographical presentation of an often rapidly acquired 4D dataset, with a lesser degree of information inside the depth of the 3D volume of data compared to high-resolution 3D data volumes.
2. *Multiplanar reconstruction (MPR):* three perpendicular planes (axial, coronal, and longitudinal) are displayed simultaneously (Figs. 6.6, 6.7) and can be moved and rotated to allow the operator to infinitely vary the different section parameters and visualize the lesion at different angles (Fig. 6.8).
3. *Volume render mode (VRM):* this is a special feature that can be applied to high-resolution 3D-US [7]. Under normal circumstances, an US image has no depth information because the lateral resolution of the image must be kept as high as possible. The image may be compared to looking at a photographic image on a piece of paper. Three-dimensional US does not change this fact. All three of the surfaces visible on the screen when viewing a 3D volume also have no depth information. This can be compared to looking at a cardboard box from the outside. The contents of the box remain unknown. Volume rendering changes the depth information

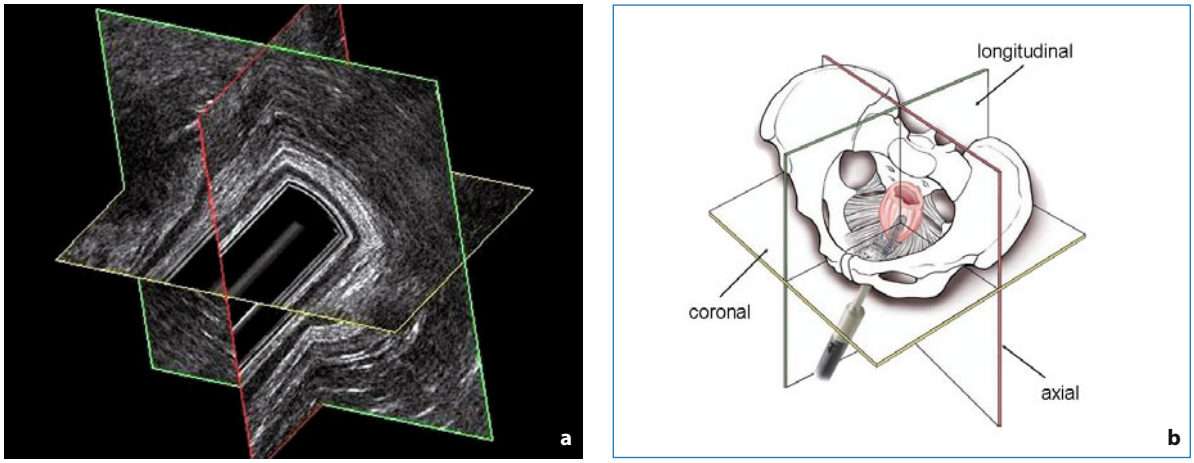

Fig. 6.6 Three-dimensional endovaginal ultrasonography with multiplanar reconstruction. **a** The axial, coronal, and longitudinal planes are simultaneously displayed in the same ultrasonographic image. **b** Schematic illustration. Image obtained using the 2050 probe (B-K Medical). Reproduced from [3]

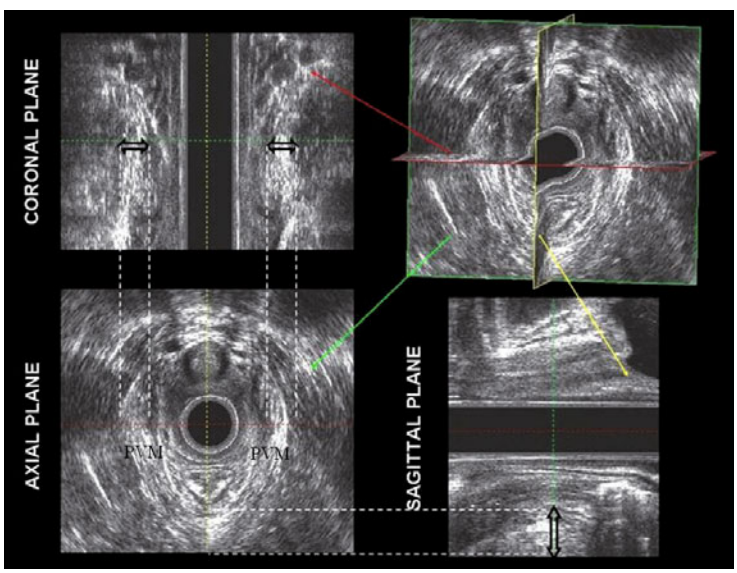

Fig. 6.7 Three-dimensional endovaginal ultrasonography with multiplanar reconstruction. The pubovisceral muscle (PVM) thickness can be measured at the 3 o'clock and 9 o'clock positions on the coronal plane, and at the 6 o'clock position on the sagittal plane (*arrows*)

of a 3D data volume so information inside the cube is reconstructed to some extent (Fig. 6.9). This technique uses a ray tracing model as its basic operation. A beam is projected from each point on the viewing screen (the display) back into and through the volume data. As the beam passes through the volume data, it reaches the different elements (voxels) in the dataset. Depending on the various render mode settings, the data from each voxel may be discarded, may be used to modify the existing value of the beam, or may be stored for reference to the next voxel and used in a filtering calculation. All of these calculations result in the current color or intensity of the beam being modified in some way. In normal VRM, the following four different postprocessing display parameters can be used [7]:

a. *opacity*: sets the relative transparency of the volume. The higher the value, the further into the volume the ray can travel before being terminated. Because of accumulated brightness as the ray traverses the volume, the net effect is to make the volume appear brighter as this control value is increased
b. *luminance*: sets the inverse of the self-luminance value for the pixels, and should be used in conjunction with the opacity control for displaying

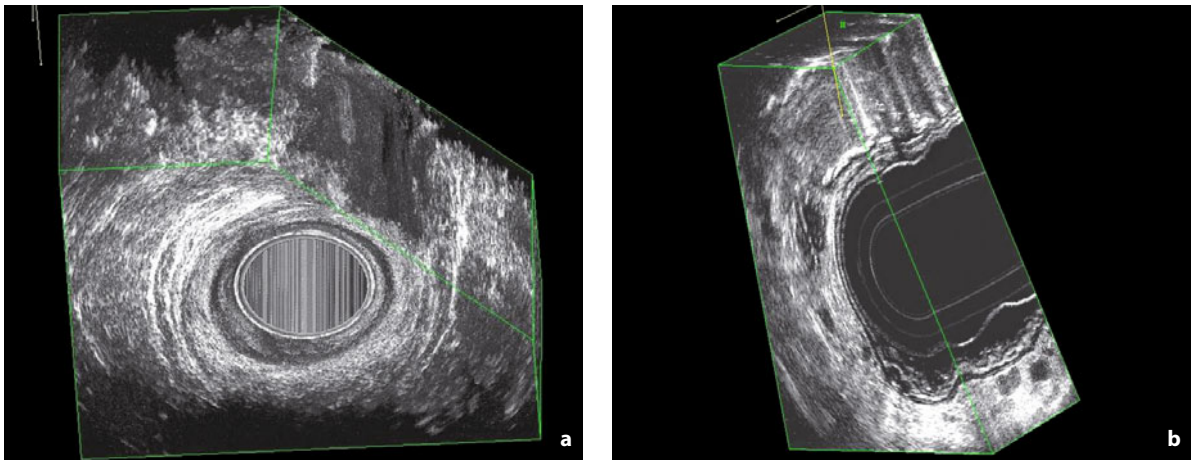

Fig. 6.8 Three-dimensional endovaginal ultrasonography with multiplanar reconstruction: oblique sections (**a**, **b**). Images obtained using the 2050 probe (B-K Medical)

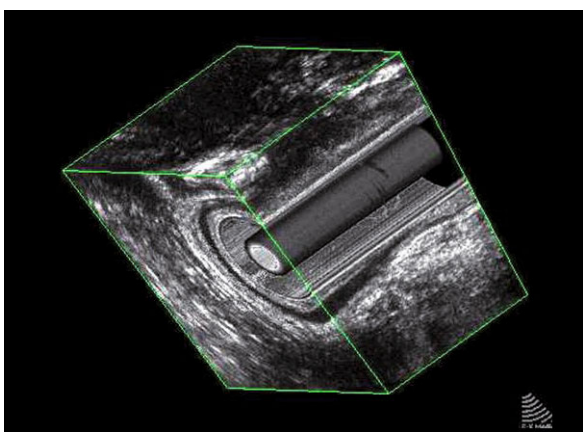

Fig. 6.9 Three-dimensional endovaginal ultrasonography with volume rendering modality. This technique changes the depth information of a 3D data volume, so information inside the cube is reconstructed to some extent

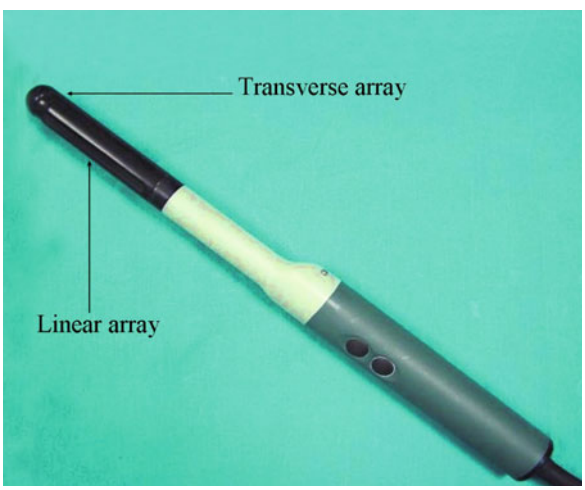

Fig. 6.10 The electronic linear transducer type 8848 (B-K Medical). This probe has a linear and a curved transverse array

certain voxel values for optimal visualization. The final image impression should be adjusted to the reader's requirements by setting the normal brightness and contrast controls

c. *thickness*: sets an upper limit to the penetration of the rays into the volume. This value is used in conjunction with the opacity parameter to determine when the ray traversal is terminated. Increasing the thickness setting allows deeper penetration, and the result is often a slightly smoother presentation together with a significant increase in the visual depth impression of a lesion
d. *filter*: sets the lower threshold value for pixel intensities. Pixel values less than the filter value are not included in determining the intensity of the final ray value. In normal VRM, the rendering mode stops each ray when the value found reaches a specified value of opacity. This is affected by the setting of some of the controls (opacity, thickness, and to some extent luminance).

Endovaginal US can also be performed with an electronic linear transducer 21 mm in diameter (type 8848, B-K Medical), frequency range 5–12 MHz, focal range 3–60 mm. The 8848 is a biplane transducer with linear and curved transverse arrays (Fig. 6.10). The linear array of this transducer has a long contact surface (65 × 5.5 mm) and a 90° imaging orientation to the longitudinal axis. A computer-controlled acquisition of 350 parallel longitudinal 2D images in 25 s is obtained by connecting

Fig. 6.11 The 180° rotational mover for 3D motorized acquisition is connected to the transducer type 8848 (B-K Medical) by using a magnetic disk

the probe to a 180° rotation mover (UAO513 B-K Medical) (Fig. 6.11). For assessment of the anterior compartment, rotation is performed from the right side (9 o'clock position) to the left side (3 o'clock position) of the patient, and for assessment of the posterior compartment from the 3 o'clock to the 9 o'clock position (Fig. 6.12).

The 8848 transducer also provides evaluation of the vascular pattern of the urethra by the use of color Doppler, and allows a dynamic assessment to be performed by asking the patient to squeeze, or to make a Valsalva maneuver.

6.3 3D Ultrasonographic Anatomy of the Pelvic Floor

No patient preparation is required. We recommend the patient has a comfortable volume of urine in the bladder. No rectal or vaginal contrast is used. The patient is placed in dorsal lithotomy and the probe is inserted into the vagina in a neutral position to avoid excessive pressure on surrounding structures that might distort the anatomy.

Assessment is initially performed with the 2050 transducer to provide a topographical overview of the pelvic floor anatomy (Fig. 6.13). The 3D-data automatic acquisition starts slightly above the bladder neck to end below the external meatus of the urethra. We define four standard levels of assessment in the axial plane (Fig. 6.14) [8].

- *Level I*: at the highest level the bladder base can be visualized on the screen at the 12 o'clock position and the inferior one-third of the rectum at the 6 o'clock position.
- *Level II*: corresponds to the bladder neck, the intramural region of the urethra, and the anorectal junction.
- *Level III*: corresponds to the midurethra and to the upper one-third of the anal canal. To facilitate assessment of the position of these structures and for evaluation of the symmetry between the urethra and

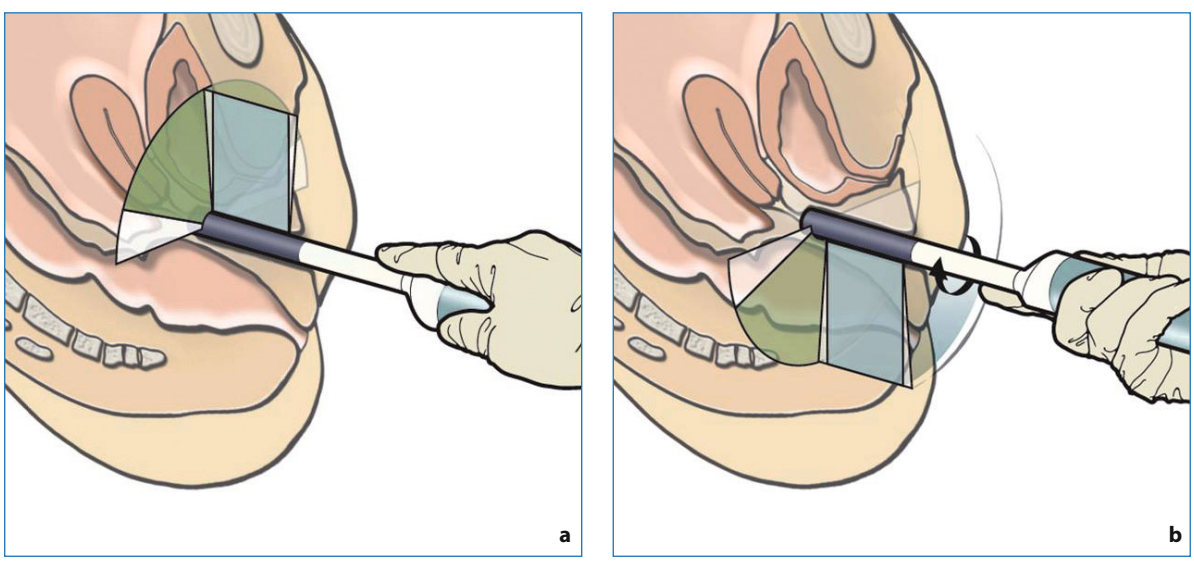

Fig. 6.12 Schematic illustrations of the technique of endovaginal ultrasonography performed by 8848 probe (B-K Medical) for the assessment of the anterior (**a**) and posterior compartment (**b**)

anal canal, a geometric reference point, termed "gothic arch", is defined at the 12 o'clock position, specifically at the point where the inferior branches of the pubic bone join at the symphysis pubis (SP). At this level, the muscles of the lateral compartment can be accurately evaluated. The puboviscerali muscle (PVM) is completely visualized as a multilayer highly echoic sling, lying posteriorly to the anal canal and attaching to the pubic bone (Fig. 6.15) [9, 10]. The fiber directions of the PVM are oblique to the axial scan plane, such that the entire muscle loop is not visible in any one slice. For this reason, we use a plane parallel to the PVM, tilting the reconstructed axial plane from the most protruding surface of the SP, anteriorly, to the lowest border of the PVM surrounding the anus posteriorly (Fig. 6.16). The thickness of the PVM can be measured in the coronal plane at the 3 o'clock (left branch) and 9

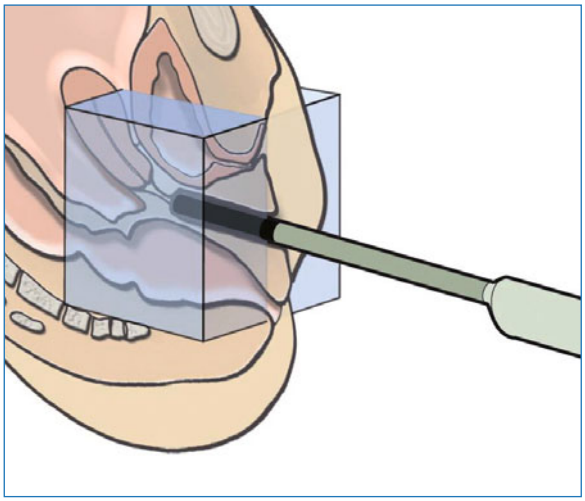

Fig. 6.13 Schematic illustration of the technique of 3D endovaginal ultrasonography performed by 2050 probe (B-K Medical) for assessment of the pelvic floor

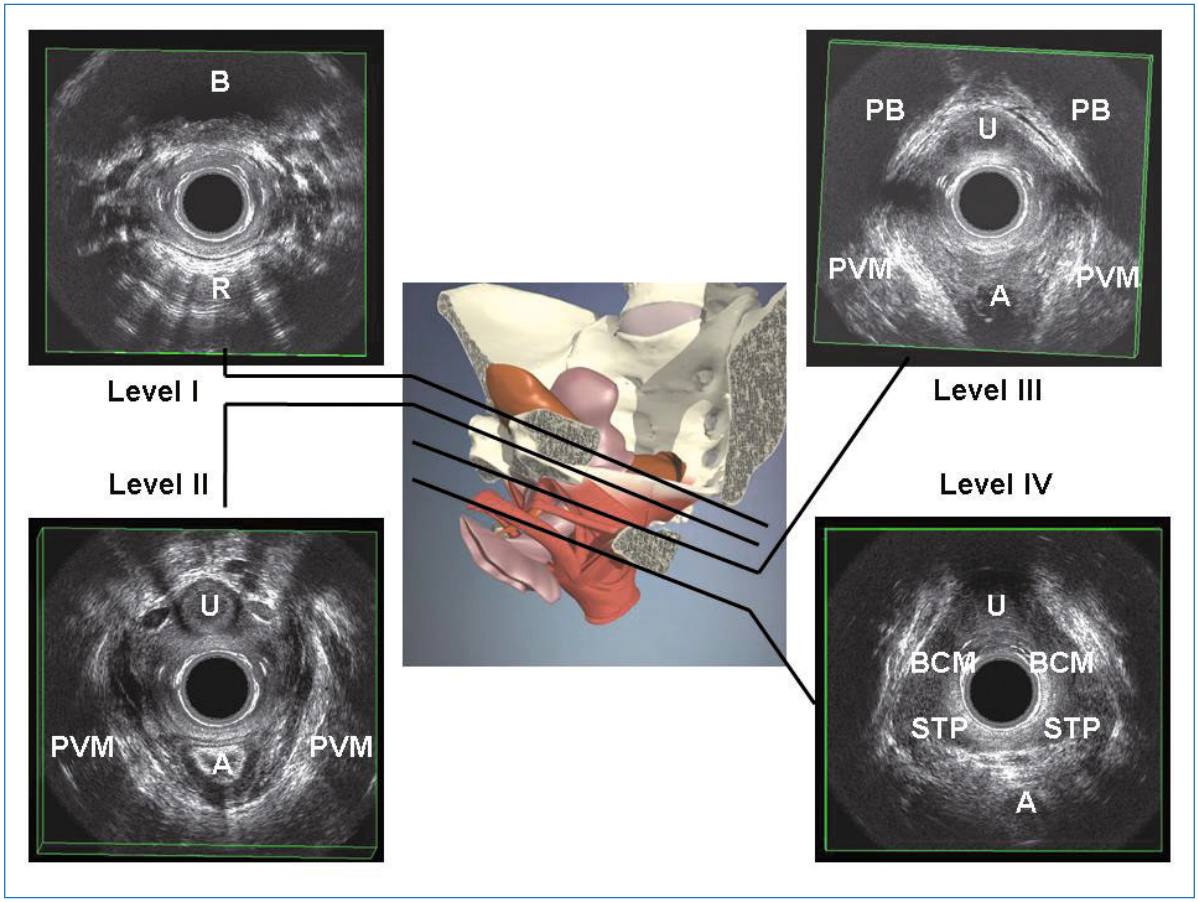

Fig. 6.14 Four standard levels of assessment of the female pelvic floor with endovaginal ultrasound (2050 transducer, B-K Medical). Right side of the image is left side of the patient. *A*, anal canal; *B*, bladder; *BCM*, bulbocavernosus muscle; *PB*, pubic bone; *PVM*, puboviscerel muscle; *R*, rectum; *STP*, superficial transverse perinei muscle; *U*, urethra

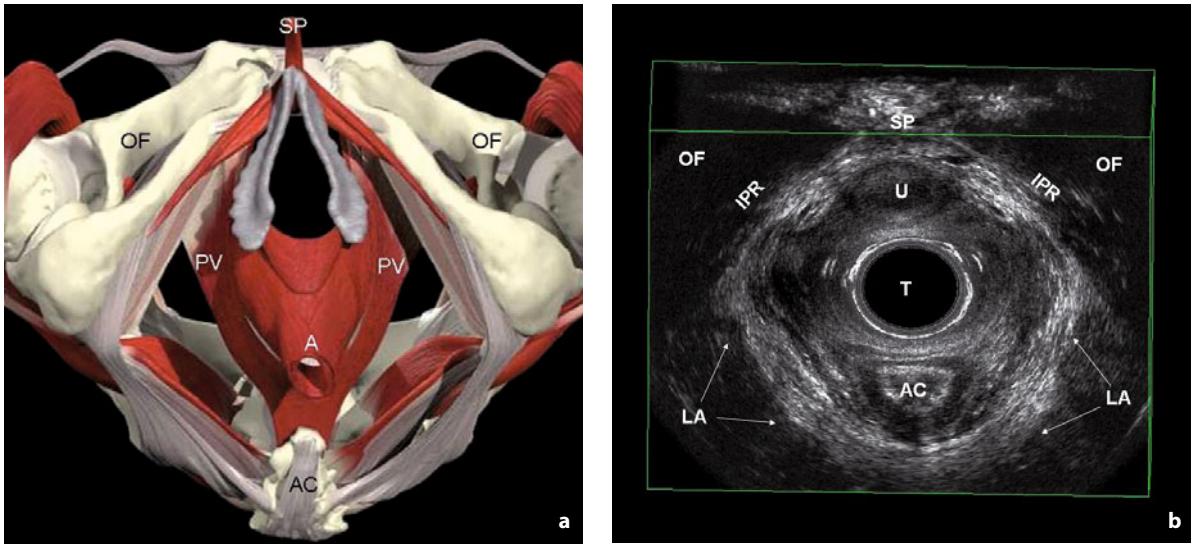

Fig. 6.15 Female pelvic floor: Level III. **a** Schematic illustration (© Primal Pictures Ltd., with permission). **b** Ultrasonographic images obtained by 2050 probe (B-K Medical). Reference point of symmetry between the urethra and anal canal is the symphysis pubis. *A*, anal canal; *AC*, anococcygeal ligament; *IPR*, inferior pubic rami; *LA*, levator ani; *OF*, obturator foramen; *PV*, pubovisceral muscle; *SP*, symphysis pubis; *T*, transducer; *U*, urethra

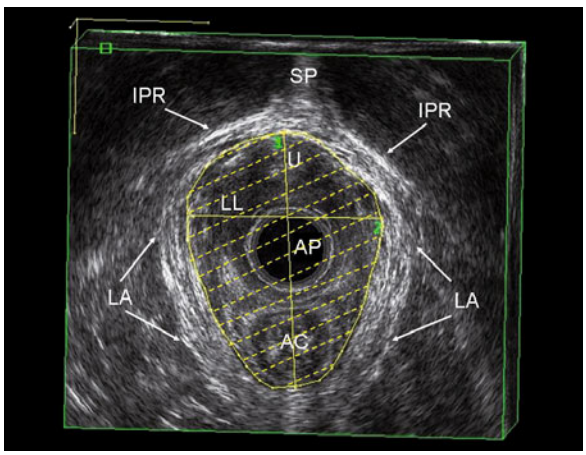

Fig. 6.16 The levator hiatus (*LH*) indices are measured at level III. In this 28-year-old female the anteroposterior diameter (*AP*) was 42.6 mm, the transverse diameter (*LL*) was 32.2 mm and LH area was 12.8 cm^2 . Scan obtained by 2050 transducer. *AC*, anal canal; *IPR*, inferior pubic rami; *LA*, levator ani; *SP*, symphysis pubis; *U*, urethra

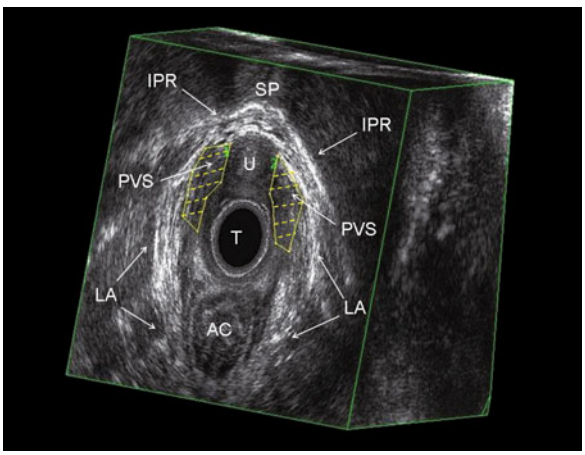

Fig. 6.17 Paravaginal spaces (*PVS*) measured on the right (*1*) and left (*2*) sides (1.69 cm^2 and 1.55 cm^2, respectively). Scan obtained by 2050 transducer (*T*) (B-K Medical). *AC*, anal canal; *IPR*, inferior pubic rami; *LA*, levator ani; *SP*, symphysis pubis; *U*, urethra

o'clock position (right branch), and in the sagittal plane at the 6 o'clock position (Fig. 6.7). In the same tilted axial plane, levator hiatus (LH) measurements are determined. The distance between the inferior margin of the SP and the inner margin of the PVM is defined as the anteroposterior (AP) diameter of the LH. The transverse diameter of the LH is measured between the inner margins of the lateral branches of the PVM at the level of their attachment to the pubic bone. The levator hiatus area can also be calculated (Fig. 6.16). In the same scan, we determine the area of the paravaginal spaces, located between the lateral border of the vaginal wall and the medial border of the PVM (Fig. 6.17).

In a study on 20 nulliparous females we found that increasing LH area was correlated with an increase in LH anteroposterior diameter ($\rho = 0.7$; $P = 0.0007$) and LH laterolateral (LL) diameter

Table 6.1 Biometric indices of the relevant pelvic floor structures assessed by 3D-EVUS with 360° rotating transducer [8]

Parameter	Plane of examination	Mean	SD
Levator hiatus			
AP diameter (cm)	Tilted axial plane	4.85	0.46
LL diameter (cm)	Tilted axial plane	3.29	0.18
Area (cm^2)	Tilted axial plane	12.0	1.70
Paravaginal space (cm^2)			
Left side	Tilted axial plane	1.05	0.10
Right side	Tilted axial plane	1.05	0.10
Pubovisceral muscle thickness (mm)			
3 o'clock	Coronal plane	6.0	0.5
9 o'clock	Coronal plane	6.0	0.6
6 o'clock	Sagittal plane	5.5	0.7
Urogenital hiatus			
AP diameter (cm)	Tilted axial plane	3.0	0.45
Ischiocavernosus muscle length (cm)			
Left side	Tilted axial plane	3.32	0.22
Right side	Tilted axial plane	3.32	0.27
Superficial transverse perinei muscle length (cm)			
Left side	Tilted axial plane	2.5	0.20
Right side	Tilted axial plane	2.6	0.18
Bulbocavernosus muscles thickness (mm)			
Left side	Tilted axial plane	3.15	0.40
Right side	Tilted axial plane	3.11	0.28

AP, anteroposterior; *LL*, laterolateral; *SD*, standard deviation

($\rho = 0.58$; $P = 0.008$). Statistically significant correlations were also found between LH area and age ($\rho = 0.5$; $P = 0.03$) and between the area of the paravaginal spaces and age ($\rho = 0.7$; $P = 0.00038$) (Table 6.1) [8].

- *Level IV:* at the outer level, the superficial perineal muscles, the perineal body, the distal urethra, and the middle and inferior one-third of the anal canal can be evaluated. To visualize these structures in their entirety, the reconstructed axial plane is tilted from the most protruding surface of the SP anteriorly, to the ischiopubic rami laterally so that the different insertion points of the perineal muscles can be seen (Fig. 6.18). The ischiocavernosus muscles are visualized as two hypoechoic bands extending from the SP to the ischiopubic rami. The superficial transverse perinei muscles (STP) are visualized as two hypoechoic bands lying transversely between the ischial tuberosity and the perineal body. The bulbocavernosus muscles appear as an oval hypoechoic structure surrounding the vaginal wall and extending from the SP to the perineal body.

In the same scan, we can determine the anteroposterior diameter of the urogenital hiatus (UGH), corresponding to the SP–perineal body distance [11]. We have also found that the UGH AP diameter significantly correlated with LH area ($\rho = 0.58$; $P = 0.008$) (Table 6.1) [8].

6.3.1 Assessment of the Anterior Compartment

Using the sagittal plane of the 3D volume acquired by 2050 transducer, we can obtain a longitudinal view of the anterior compartment and can assess the bladder neck and the urethra (Fig. 6.19). Additional information is provided by using the 8848 transducer (Fig. 6.10) [8]. Assessment of the anterior compartment in the midsagittal section includes measurements of the length (from the bladder neck to the external urethral orifice) and thickness of the urethra, bladder–symphysis distance (from the bladder neck to the lowest margin of the SP), rhabdosphincter (RS) length and thickness,

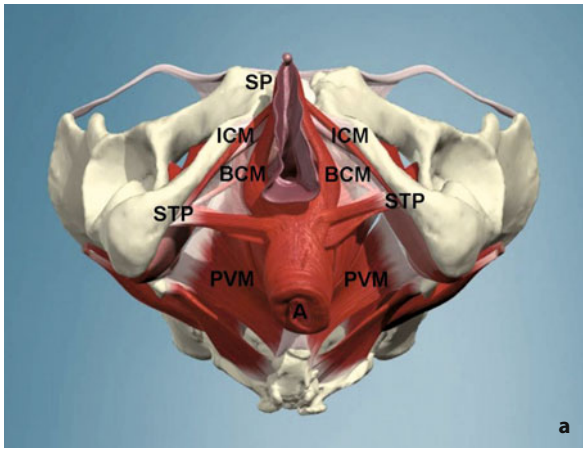

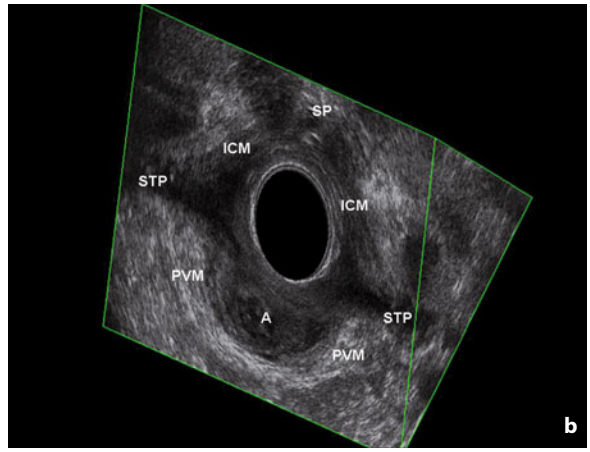

Fig. 6.18 Superficial structures of the lower pelvis: Level IV. **a** Schematic illustration (© Primal Pictures Ltd., with permission). **b** Ultrasonographic image obtained by 2050 transducer (B-K Medical). *A*, anal canal; *BCM*, bulbocavernosus muscles; *ICM*, ischiocavernosus muscles; *PVM*, pubovisceral muscle; *SP*, symphysis pubis; *STP*, superficial transverse perinei muscle

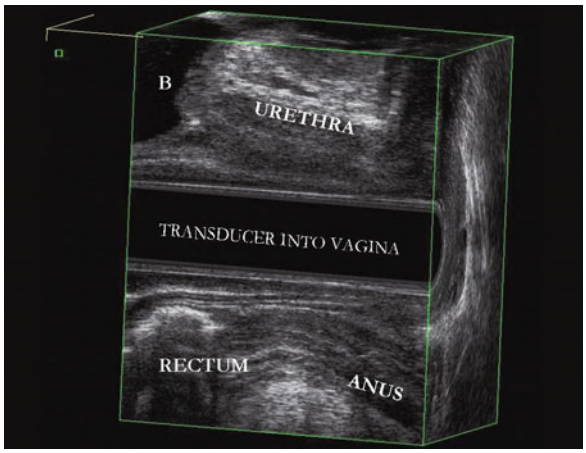

Fig. 6.19 Three-dimensional reconstruction of the longitudinal plane allows assessment of the anterior and posterior compartments. *B*, bladder. Image obtained by 2050 transducer (B-K Medical)

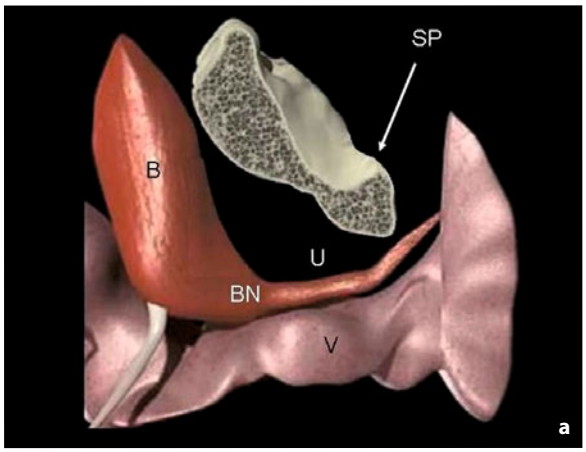

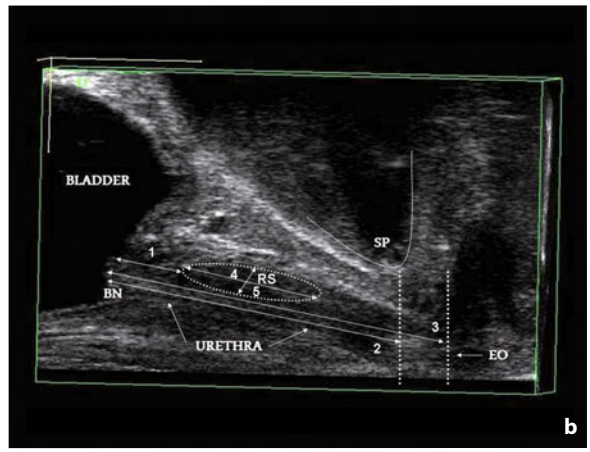

Fig. 6.20 Longitudinal view of the anterior compartment. **a** Schematic illustration (© Primal Pictures Ltd., with permission). **b** Ultrasonographic image obtained by 8848 transducer (B-K Medical) using the linear array. Measurements include: bladder neck-rhabdosphincter distance (*1*), bladder-symphysis distance (*2*), urethral length (*3*), rhabdosphincter length (*4*) and thickness (*5*). *B*, bladder; *BN*, bladder neck; *EO*, external urethral orifice; *RS*, rhabdosphincter; *SP*, symphysis pubis; *U*, urethra; *V,* vagina

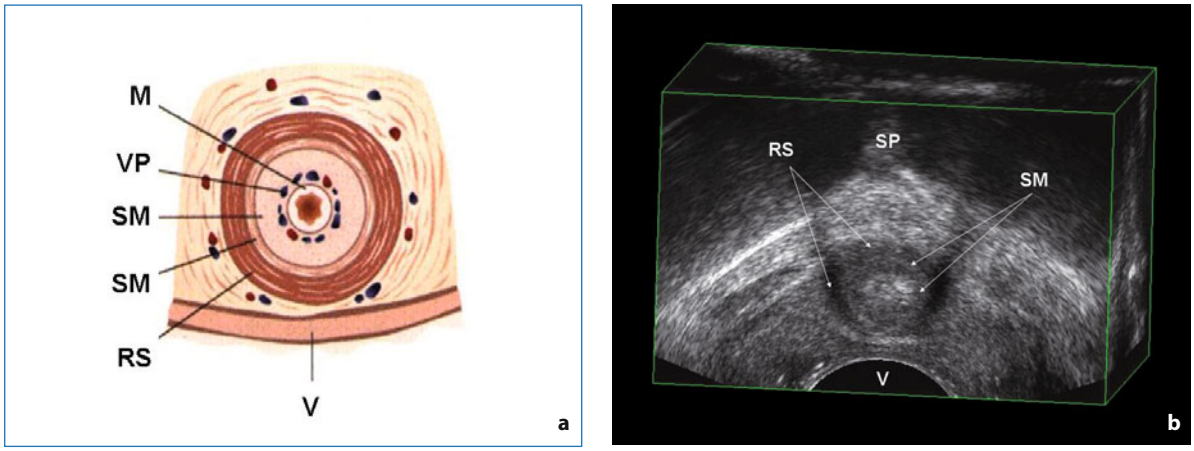

Fig. 6.21 **a** Schematic representation of the midurethra in the axial plane. **b** Ultrasonographic image obtained by 8848 transducer (B-K Medical) using the axial array. Rhabdosphincter (*RS*) appears as a slightly echoic structure overlapping a more echoic smooth urethral muscle (*SM*). *M,* mucosa; *SP*, symphysis pubis; *V,* vagina; *VP*, vascular plexus

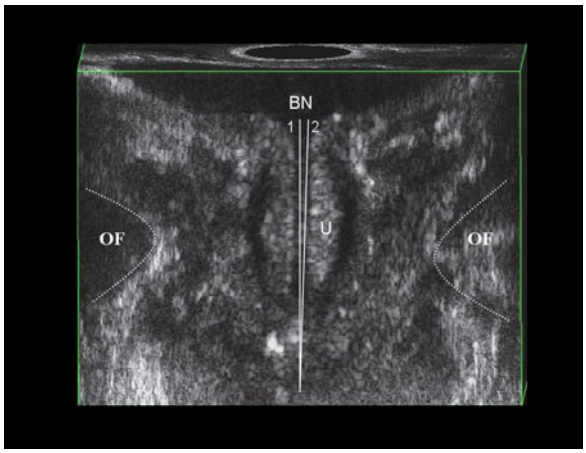

Fig. 6.22 Coronal view of the urethra (*U*). In this plane, the omega angle, formed by the vertical line passing through the bladder neck (*BN*) (*1*) and the long axis of the urethra (*2*), can be measured. Image obtained by 8848 transducer. *OF*, obturator foramen

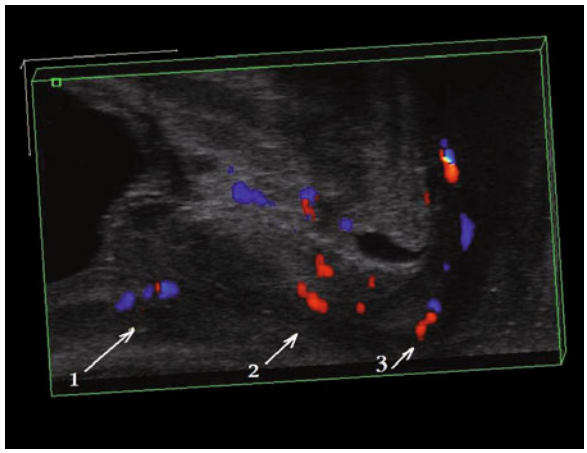

Fig. 6.23 Vessels supporting the urethral complex form three levels (1.intramural part of the urethra, 2.midurethra, 3.distal part of the urethra) in the longitudinal plane. Scan obtained by 8848 transducer (B-K Medical) using the linear array

and the distance between the bladder neck and the RS (Fig. 6.20). The striated urethral sphincter (RS) starts in the upper part of the urethra approximately 9.1 mm (range: ± 0.94 mm) from the urinary bladder neck. In transverse section it has a typical omega shape, surrounding the ventral and lateral sides of the midurethra and creating a raphe connected to the anterior vaginal wall. Its echogenicity is slightly lower than that of smooth urethral muscle (Fig. 6.21).

In our study on 20 nulliparous females, significant correlations were found among the following parameters: urethral width with urethral length ($\rho = 0.65$; $P = 0.002$) and urethral thickness ($\rho = 0.5$; $P = 0.02$); urethral volume with urethral thickness ($\rho = 0.7$; $P = 0.002$), urethral width ($\rho = 0.87$; $P = 0.0001$), urethral length ($\rho = 0.75$; $P = 0.00005$) and RS volume ($\rho = 0.5$; $P = 0.03$) [8]. The position of the urethra is determined in the reconstructed coronal plane by measuring the angle that we term "omega angle", between the vertical line passing through the bladder neck and the long axis of the urethra (Fig. 6.22).

The urethra is surrounded by connective tissue containing numerous vessels. In the reconstructed longitudinal plane these vessels appear to form three levels (Fig. 6.23). The first level, situated cranially, is seen below the urinary bladder neck. The second level is situated in the middle region of the urethra penetrating from the ventral side to reach the RS. The vessels pen-

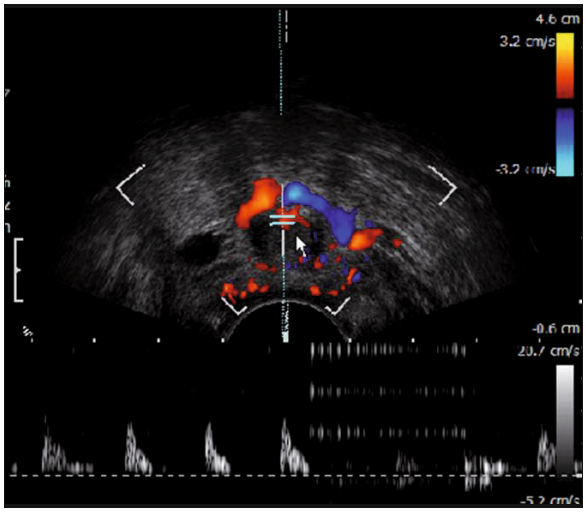

Fig. 6.24 Vascularity of the urethra assessed in the axial plane by color Doppler. Scan obtained by 8848 transducer (B-K Medical)

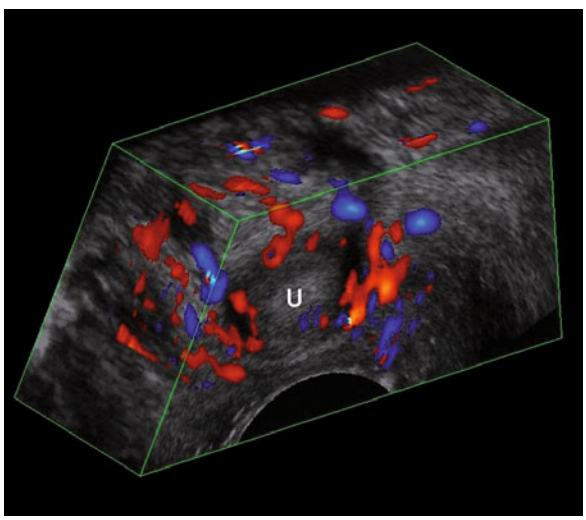

Fig. 6.25 Three-dimensional color Doppler imaging. Spatial distribution of the urethral vessels. Image obtained by 8848 transducer (B-K Medical). *U*, urethra

etrating here, on transverse section, have a typical "V" shape (Fig. 6.24). The third and lowest level is situated below the lower margin of the SP, in the area of the external ostium.

Using 3D color Doppler imaging, we can observe the global vascularization of the urethra (Fig. 6.25). It is possible to visualize the spatial distribution of blood flow, to demonstrate vessel continuity and vessel branching in different planes, and to evaluate the pattern of vascularization (density of vessels, branching, caliber changes and tortuosity).

6.3.2 Assessment of the Lateral Compartment

The area posterior to the pubic bone is dense with bands of intertwined levator ani muscles which defy conventional description of the levator ani being made up of the puborectalis, pubococcygeus, and iliococcygeus muscles. The anatomy of distal subdivisions of the levator ani muscle was further described in a recent study [12]. Using a nomenclature based on the attachment points of different subdivisions of the levator ani muscles, the muscles posterior to the pubic bone are identified as the pubovaginalis, puboanalis, and puboperinealis as the subdivisions of the PVM [13]. Margulies et al demonstrated excellent reliability and reproducibility in visualizing major portions of the levator ani in nulliparous volunteers with magnetic resonance imaging (MRI) [14]. However, because the puboanalis, pubovaginalis, and puboperinealis are small, they have proved to be difficult to visualize in the rigid axial, coronal, and sagittal views of MRI.

Shobeiri et al [15] identified the subdivisions of the distal levator ani as seen on 3D-EVUS in cadaveric dissections. Endovaginal scanning was performed as described earlier in this chapter. Echogenic structures suspicious for being STP, pubovaginalis, puboperinealis, puboanalis, puborectalis, and iliococcygeus muscles were tagged with biopsy needles (MPM Medical, Elmwood Park, NJ) and marked with 1 mL indigo carmine dye for localization. Additionally, any other unknown structures and possible defects were tagged in the same manner (Fig. 6.26). After each pelvis was scanned with US, the findings were recorded digitally, and each pelvis

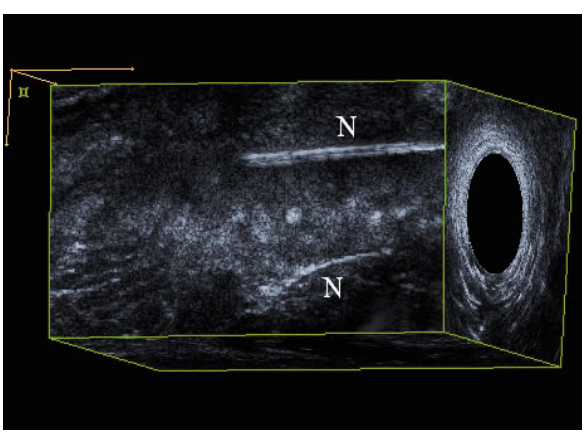

Fig. 6.26 Ultrasound needle (*N*) localization of muscles. Sagittal view of two needles inserted into the iliococcygeus muscle. Image obtained by 2050 transducer (B-K Medical)

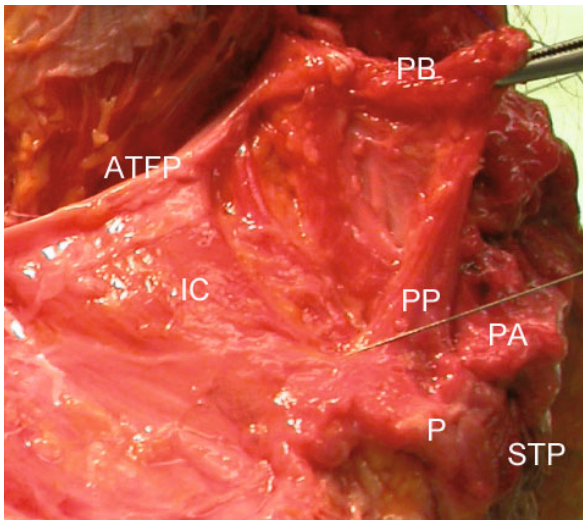

Fig. 6.27 Gross cadaveric dissection. A needle is seen inserted into the puboperinealis muscle (*PP*). The other structures are identified: *ATFP*, arcus tendineus fascia pelvis; *IC*, iliococcygeus muscle; *PA*, puboanalis muscle; *PB*, pubic bone or pubic bone insertion; *P*, perineum; *STP*, superficial transverse perinei muscle

dissected to locate each of the numbered needles in all the cadaveric specimens (Fig. 6.27) [15].

In the US imaging and the correlative dissections of the fresh-frozen pelvis, the STP was the first muscle visualized (Fig. 6.28). Immediately cephalad to it was the puboperinealis insertion into the perineal body. In the dissections, the puboanalis was located deep and lateral to the puboperinealis and had a wide base inserting itself into the anorectal fibers. Puboanalis fibers intermixed with lateral supportive fibers of the rectum to form the posterior arcus, which in turn fused with laterally located fibers of the iliococcygeus [16]. The pubovaginalis was a short band 3 cm cephalad to the ischiopubic rami, causing an indentation in the anterior vaginal epithelium. The puborectalis insertion was lateral, wrapping itself around the rectum 3 cm cephalad to the anus. By US, the puboperinealis had mixed echogenicity and was located immediately cephalad to superficial transverse perinei. The puboanalis was identified as a triangular hypoechoic area lateral to puboperinealis. The pubovaginalis was identified as dense muscular bands at the level of the midurethra in cadavers, and as hypoechoic areas causing heart-shaped angulation of the anterior vaginal mucosa. All these structures and the iliococcygeus were accurately identified by needle identification during 3D-EVUS, and authenticated by gross dissection (Fig. 6.28) [15].

Shobeiri et al [15] also performed the 3D scans in 50 nulliparous volunteers to develop a scoring system for visualization of the pelvic floor muscles. The characteristic features of each of the five separate levator subdivisions were determined on a three-level system. Level 1 contained the muscles that insert into the perineal body, namely the STP, puboperinealis, and puboanalis muscles. Superficial transverse perinei served as the reference point. Level 2 contained the attachment of the pubovaginalis, puboperinealis, puboanalis, puborectalis, and iliococcygeus to the pubic bone. Level 3 contained subdivisions visible cephalad to the inferior pubic ramus, namely the iliococcygeus which winged out towards the ischial spine. The visualization of the pubococcygeus was debatable, and since this structure was not reliably visualized during pelvic floor dissection, it was not included. Using this system (muscle subdivisions "visible" or "not visible" at three levels), they calculated the inter-rater reliability. There was 98% (95% CI: 0.92–1), 96% (95% CI: 0.95–0.99), and 92% (95% CI: 0.88–0.95) agreement for level 1, 2, and 3 muscles respectively. κ values for agreement were calculated for individual muscles as follows: STP and puborectalis, $\kappa = 1$ (excellent agreement); puboperinealis, pubovaginalis, and puboanalis: $\kappa = 0.645$ (good agreement); iliococcygeus, $\kappa = 0.9$ (excellent agreement) [15].

6.3.3 Assessment of the Posterior Compartment

The posterior compartment is evaluated by using the axial, sagittal, and coronal planes of the 3D volume acquired by 2050 (Fig. 6.19) or 8848 transducers (Fig. 6.12) [8]. Assessment includes measurements of the internal (IAS) and external anal sphincters (EAS). In the axial plane the IAS appears as a concentric hypoechoic ring surrounding a more echogenic central mucosa, and the EAS appears as a concentric band of mixed echogenicity surrounding the IAS (Fig. 6.29). The thickness of the internal and external sphincters is taken in the coronal plane at the 3 o'clock and 9 o'clock positions. An echogenic disruption is defined as a gap. The location of any defect is described using a clock-face notation. The longitudinal plane allows examination of the perineal body, appearing as a triangular-shaped, slightly hyperechoic structure anterior to the anal sphincter, and of the rectovaginal septum (RVS), visualized as a three-layer-structure (hyperechoic,

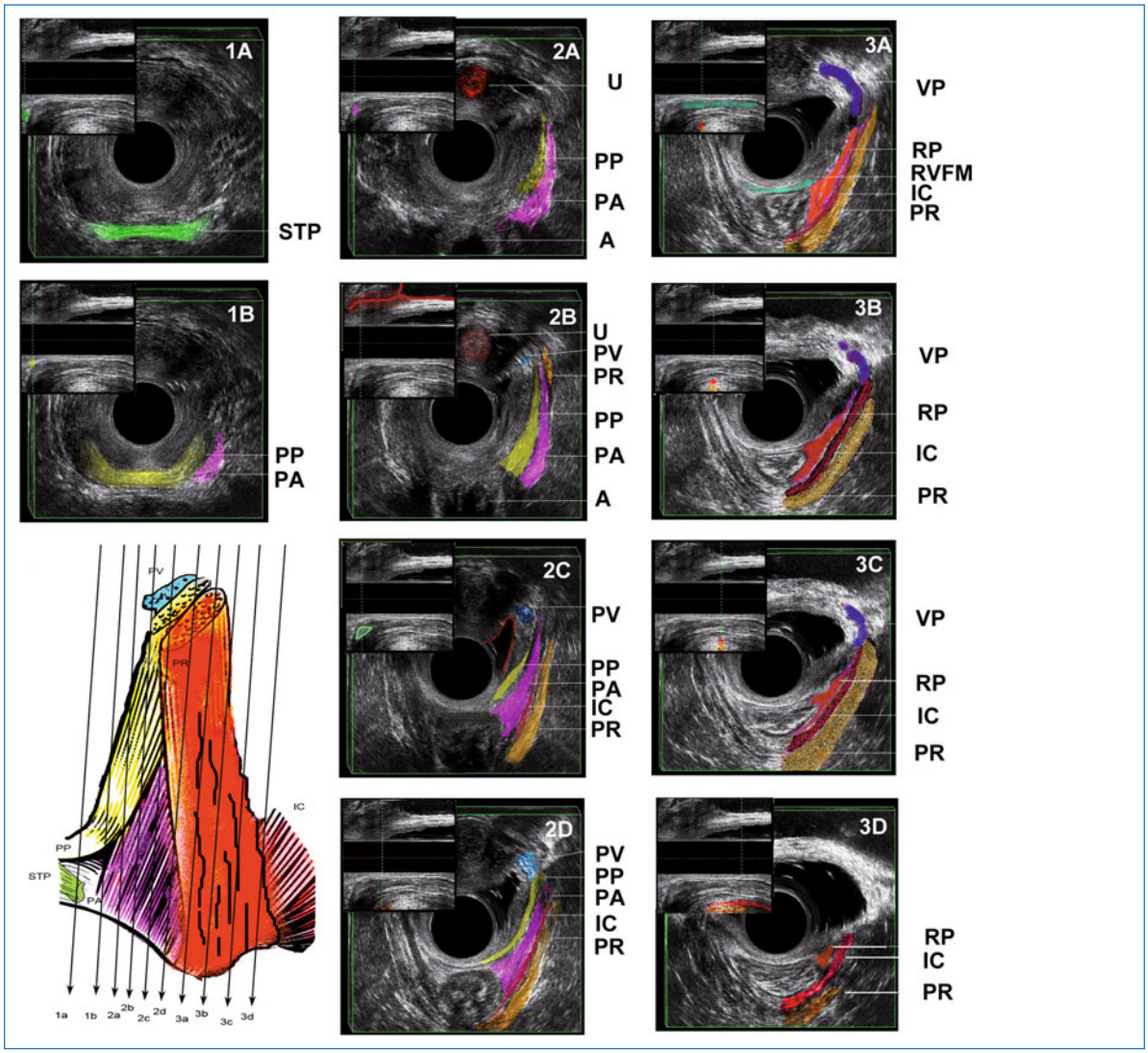

Fig. 6.28 Drawing (bottom left): the relative position of the levator ani subdivisions during ultrasound imaging: Levels 1A–3D are identified in the individual panels. Midline structures are identified in lateral views with corresponding colors in the picture insert at the upper left corner of the ultrasound images at each level. The dotted green vertical line in the insert corresponds to the relative position in the vagina where the image is obtained. Level 1A: at 0 cm, the first muscle seen is the superficial transverse perinei muscle (*STP*; green) with mixed echogenicity. Level 1B: immediately cephalad to the superficial transverse perinei is the puboperinealis muscle (*PP*; yellow) that can be traced to pubic bone with manipulation of the 3D cube. It comes in at a 45° angle as a mixed echoic band to join the perineal body. Lateral to it, the puboanalis muscle (*PA*, pink) is seen as a hypoechoic triangle. Level 2A: this level marks the attachment of the muscles to the pubic arch. The external urethral meatus is visible (dark red). The puboperinealis and puboanalis insertions are highlighted (*A*, anus; *U*, urethra). Level 2B: the pubovaginalis (*PV*, blue) and puborectalis muscles (*PR*, mustard) insertions come into view. The urethra (*U*) and the bladder are outlined (red) in the lateral view. Level 2C: the heart-shaped vaginal sulcus (outlined in red) marks the pubovaginalis insertion. Iliococcygeus (*IC*) fibers (red) come into view. The perineal body is outlined in the lateral view. Level 2D: the puboanalis (*PA*) is starting to thin out. The puborectalis (*PR*) is seen in the lateral view. Level 3A: the puboperinealis (*PP*) and puboanalis (*PA*) become obscure. Anatomically, the puboanalis becomes a thick fibromuscularis layer forming a tendineus sheet, the rectal pillar (*RP*). The perivesical venous plexus (*VP*) is prominent (purple). The rectovaginal fibromuscularis (*RVFM*, green) is shown in sagittal view as a continuous mixed echogenic structure approaching the perineal body and laterally attaching to the RP. Level 3B: the rectal pillar (orange) is easily seen. The iliococcygeus (*IC*) becomes prominent and widens. Level 3C: the iliococcygeus (*IC*) widens further and inserts into the arcus tendineus fascia pelvis. Level 3D: the puborectalis (*PR*) fades out of view. The puborectalis (mustard) and iliococcygeus (red) are outlined in the lateral view showing their entire course

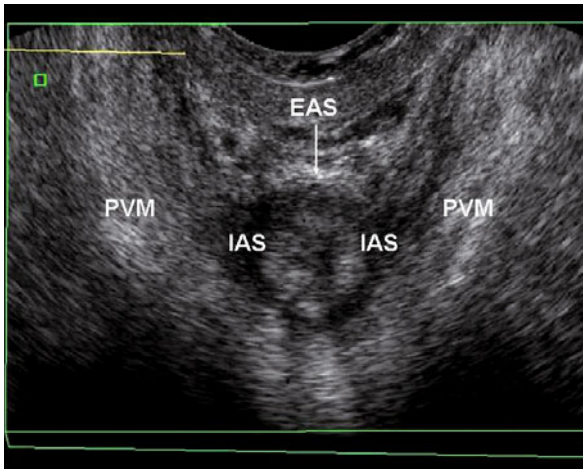

Fig. 6.29 Axial view of the anal complex obtained by 8848 transducer (B-K Medical) using the transverse array. The external anal sphincter (*EAS*) appears as a hyperechoic ring surrounding the hypoechoic ring of the internal anal sphincter (*IAS*); *PVM*, pubovisceral muscle

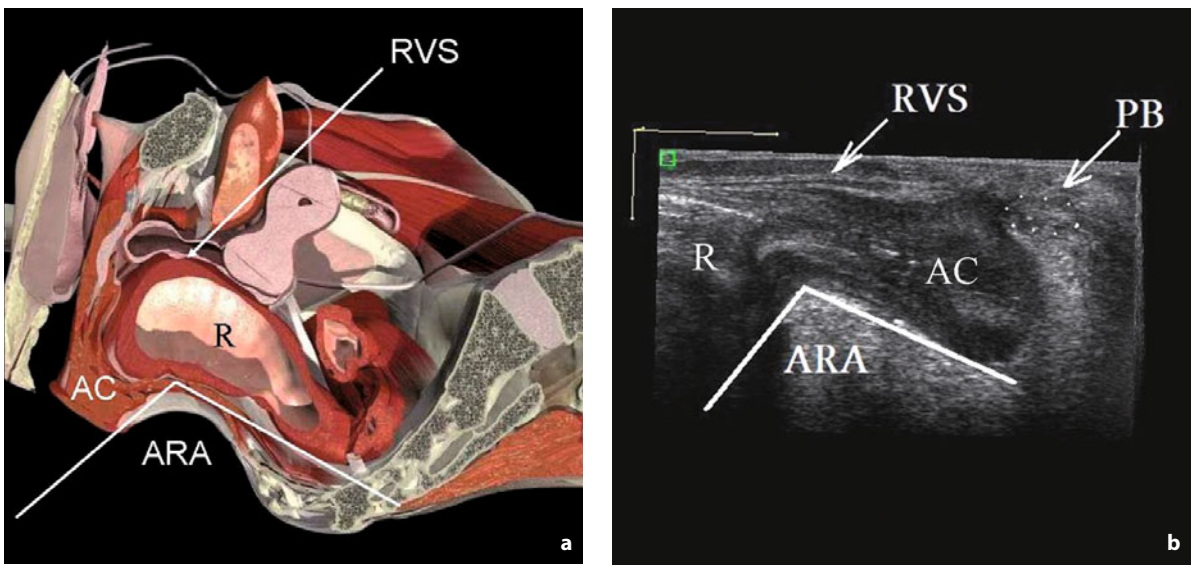

Fig. 6.30 Longitudinal view of the posterior compartment. **a** Schematic illustration (© Primal Pictures Ltd., with permission). **b** Ultrasonographic image obtained by 8848 transducer (B-K Medical) using the linear array. *AC*, anal canal; *ARA*, anorectal angle; *PB*, perineal body; *R,* rectum; *RVS*, rectovaginal septum

hypoechoic, and hyperechoic layers) between the external margin of the vagina and the external part of the rectal wall (Fig. 6.30). An RVS defect is defined as a discontinuity in this echographic pattern. In the midsagittal plane, the anorectal angle (ARA), formed by the longitudinal axis of the anal canal and the posterior rectal wall, can also be measured.

6.4 Discussion

The pelvic floor is a 3D mechanical apparatus with a complex job description [17]. When we display a normal 2D-US cross-sectional view, there are many elements of the image that will not be correctly recognized as components of a 3D structure, or at least not perceived in their true spatial relationships. With ultrasound imaging we are usually looking at a 3D structure that contains a solid volume of echoes and which therefore does not readily translate onto a 2D projection. In routine clinical scanning, the operator forms a mental representation of the 3D anatomic or pathological structure, while viewing a large series of 2D slices interactively. In this case the operator is using manual sense information about the physical location of the individual slices in building up 3D subjective impressions.

3D- and indeed 4D-US has been promoted by different ultrasound companies for several years. The acquisition of a 3D data volume and the underlying techniques are, however, different from application to application. The pelvic floor requires extremely high-resolution 3D volumes of data for adequate and precise diagnostic evaluation. An advantage of working with high-resolution 3D-US is that the 3D image does not remain fixed, rather, it can be freely rotated, rendered, tilted, and sliced to allow the operator to infinitely vary the different section parameters and visualize the different structures at different angles to obtain the most information from the data. After data are acquired, it is possible to select coronal anterior–posterior or posterior–anterior as well as sagittal right–left views, together with any oblique image plane. The multiview function allows the reader to see up to six different and specialized views at once with multiplanar reconstruction. Three-dimensional US allows us to assess directly the different planes in which the significant anatomic structures of the pelvic floor (pelvic bones, pelvic organs, pelvic floor muscles, fascia, and ligaments) are located.

Two structures extensively evaluated by 3D-EVUS imaging are the LH and PVM [8]. Assessment of these structures is important because significant correlations have been reported between levator ani defects and increased LH size and pelvic organ descent [18] (see Chapter 37). Tilting the axial plane in the acquired 3D data volume provides a maximal transverse section of the PVM, not otherwise obtainable with conventional 2D-EVUS, thus avoiding the artifacts due to its oblique shape. Our measurements of PVM thickness (6.0 mm on both sides) were comparable with those reported by Tunn et al [19] with MRI (6.3 mm on both sides). As the lateral attachments of the PVM to the pubic bone are also clearly visualized, 3D-EVUS can be utilized to document major levator ani trauma, in a similar way to 3D translabial ultrasound (TLUS) [20] and MRI [13, 18]. This technique also allows a detailed evaluation of the levator ani subdivisions [15] which are not visualized by TLUS [20]. Although it may be argued that these subdivisions of the levator ani muscle are not important, knowing exactly which muscles are damaged may not be inconsequential in clinical practice. Many of the functions of the pelvic floor governing micturition, defecation, and intercourse are only recently understood by describing the subdivisions of the levator ani muscle. Attachments are important because the muscles exert their action by contraction. For example, a patient with defecatory dysfunction due to a detached puboperinealis will not benefit from a posterior repair. Also, reattachment of the puboperinealis does not address defecatory dysfunction due to loss of anorectal angle from a damaged puborectalis.

Biometric indices of the LH determined in the axial tilted plane in our preliminary study on 20 nulliparous females (AP diameter 4.84 cm, LL diameter 3.28 cm, hiatal area 12 cm^2) [8] were comparable to the results published by Dietz et al [9] in 49 nulliparous females with 3D-TLUS (AP diameter 4.52 cm, LL diameter 3.75 cm, hiatal area 11.25 cm^2), and Tunn et al [19] in 20 nulliparous females with MRI (AP diameter 4.1 cm, LL diameter 3.3 cm, hiatal area 12.8 cm^2). In the same tilted axial plane, the paravaginal spaces and urethral symmetry can be assessed [8]. This has clinical relevance, as a lateral paravaginal defect can be suspected when a wider paravaginal space or an asymmetry of the urethra is observed . It has been hypothesized that paravaginal defects, due to separation of the endopelvic fascia from the arcus tendineus fascia pelvis, are the underlying anatomical abnormalities in anterior vaginal wall descent [21, 22] (see Chapter 37).

Understanding the anatomy of the pelvic diaphragm is important for urogynecologists and proctologists. Damage to the perineal muscles and/or perineal body, frequently occurring during vaginal childbirth, is associated with pelvic organ prolapse [14]. As reported by Orno et al [23], these muscles cannot be visualized in their entirety by using 2D-EVUS because they originate from the walls of the pelvis and converge at the perineal body from different angles. Three-dimensional EVUS could overcome this limitation. Tilting the reconstructed axial plane from the SP, anteriorly, to the ischiopubic rami laterally, we are able to evaluate the different insertion points and to determine the dimensions of the superficial perineal muscles. In contrast with these findings, 3D-TLUS cannot properly assess the perineal structures due to the shape of the transducer, its position on the introital area, and a limited field of view of the acquired volume [22]. In the same scan, the AP diameter of the UGH can also be measured. Our study confirmed that this diameter had a positive correlation with LH area [8].

In the diagnostics of the anterior compartment, it is very important to assess the morphology and location of the urethra and to evaluate its supportive structures [19]. High-resolution 3D-EVUS gives the

opportunity to assess the urethral position in three different planes and allows the anatomy and morphology of the bladder neck and urethral complex to be quantified [8] (see Chapter 15). Biometric indices of the urethral complex determined in our study [8] were comparable to the results reported by Umek et al [6] with 3D transrectal US, with regard to both urethral thickness (11 mm on vaginal vs. 11.5 mm on rectal scans) and width (14 mm on vaginal vs. 15 mm on rectal scans) and to RS thickness (3.0 mm on vaginal vs. 2.7 mm on rectal scans) and volume (0.46 cm^3 on vaginal vs. 0.5 cm^3 on rectal scans). Additionally, the mean bladder neck–RS distance determined in our study (9.1 mm) was consistent with the measurement reported by using MRI (10 mm) [24].

The current gold standard for assessment of the posterior compartment is considered to be endoanal US (EAUS) [3, 7]. Endovaginal US offers an alternative imaging modality of the anal sphincter complex and has proven to be as accurate as EAUS [2]. Our preliminary results using this method [8] confirmed that the thickness of the anal sphincter was comparable to the measurements reported in the literature by using EAUS, TLUS, or MRI [25–27]. However, regardless of the absolute dimensions of the anal sphincters, the most relevant utility of EVUS applies in the detection of localized EAS defects when EAUS cannot depict any sphincter damage, in order to confirm or exclude EAUS findings in patients with idiopathic fecal incontinence, passive fecal incontinence, or obstructive defecation disorders. The most important advantage of EVUS compared to EAUS is the access to the longitudinal plane that allows assessment of the ARA, rectovaginal septum, and perineal body [8].

High-resolution 3D-EVUS provides a detailed assessment of the pelvic floor for both identifying and measuring specific anatomic structures and for understanding their complex spatial arrangements. It is relatively easy to perform, time efficient, correlates well with other imaging modalities, and delivers additional information on urethral complex and superficial perineal structures at the same time.

References

1. Tunn R, Petri E. Introital and transvaginal ultrasound as the main tool in the assessment of urogenital and pelvic floor dysfunction: an imaging panel and practical approach. Ultrasound Obstet Gynecol 2003;22:205–213.
2. Sultan AH, Loder PB, Bartram CI et al. Vaginal endosonography. New approach to image the undisturbed anal sphincter. Dis Colon Rectum 1994;37:1296–1299.
3. Santoro GA, Fortling B. New technical developments in endoanal and endorectal ultrasonography. In: Santoro GA, Di Falco G (eds) Benign anorectal diseases. Diagnosis with endoanal and endorectal ultrasonography and new treatment options. Springer-Verlag Italy, Milan, 2006, pp 13–26.
4. Dietz HP, Steensma AB. Posterior compartment prolapse on two-dimensional and three-dimensional pelvic floor ultrasound: the distinction between true rectocele, perineal hypermobility and enterocele. Ultrasound Obstet Gynecol 2005;26:73–77.
5. Mitterberger M, Pinggera GM, Mueller T et al. Dynamic transurethral sonography and 3-dimensional reconstruction of the rhabdosphincter and urethra: initial experience in continent and incontinent women. J Ultrasound Med 2006; 25:315–320.
6. Umek WH, Lami T, Stutterecker D et al. The urethra during pelvic floor contraction: observations on three-dimensional ultrasound. Obstet Gynecol 2002;100:796–800.
7. Santoro GA, Fortling B. The advantages of volume rendering in three-dimensional endosonography of the anorectum. Dis Colon Rectum 2007;50:359–368.
8. Santoro GA, Wieczorek AP, Stankiewicz A et al. High-resolution three-dimensional endovaginal ultrasonography in the assessment of pelvic floor anatomy: a preliminary study. Int Urogynecol J 2009;20:1213–1222.
9. Dietz HP, Shek C, Clarke B. Biometry of the pubovisceral muscle and levator hiatus by three-dimensional pelvic floor ultrasound. Ultrasound Obstet Gynecol 2005; 25:580–585.
10. Ashton-Miller JA, DeLancey JO. Functional anatomy of the female pelvic floor. Ann N Y Acad Sci 2007;1101:266–296.
11. DeLancey JOL, Hurd WW. Size of the urogenital hiatus in the levator ani muscles in normal women and women with pelvic organ prolapse. Obstet Gynecol 1998;91:364–368.
12. Shobeiri SA, Chesson RR, Gasser RF. The internal innervation and morphology of the human female levator ani muscle. Am J Obstet Gynecol 2008;199:686.e1–6.
13. Kearney R, Sawhney R, DeLancey JO. Levator ani muscle anatomy evaluated by origin-insertion pairs. Obstet Gynecol 2004;104:168–173.
14. Margulies RU, Hsu Y, Kearney R et al. Appearance of the levator ani muscle subdivisions in magnetic resonance images. Obstet Gynecol 2006;107:1064–1069.
15. Shobeiri SA, LeClaire E, Nihira MA, et al. Appearance of the levator ani muscle subdivisions in endovaginal three-dimensional ultrasonography. Obstet Gynecol 2009; 114: 66–72.
16. Lien KC, Mooney B, DeLancey JO et al. Levator ani muscle stretch induced by simulated vaginal birth. Obstet Gynecol 2004;103:31–40.
17. DeLancey JO. The hidden epidemic of pelvic floor dysfunction: achievable goals for improved prevention and treatment. Am J Obstet Gynecol 2005;192:1488–1495.
18. DeLancey JO, Morgan DM, Fenner DE et al. Comparison of levator ani muscle defects and function in women with and without pelvic organ prolapse. Obstet Gynecol 2007; 109:295–302.

19. Tunn R, DeLancey JOL, Howard D et al. Anatomic variations in the levator ani muscle, endopelvic fascia and urethra in nulliparas evaluated by magnetic resonance imaging. Am J Obstet Gynecol 2003;188:116–121.
20. Dietz HP. Quantification of major morphological abnormalities of the levator ani. Ultrasound Obstet Gynecol 2007;29:329–334.
21. DeLancey JO. Fascial and muscular abnormalities in women with urethral hypermobility and anterior vaginal wall prolapse. Am J Obstet Gynecol 2002;187:93–98.
22. Dietz HP, Steensma AB, Hastings R. Three-dimensional ultrasound imaging of the pelvic floor: the effect of parturition on paravaginal support structures. Ultrasound Obstet Gynecol 2003;21:589–595.
23. Orno AK, Marsal K, Herbst A. Ultrasonographic anatomy of perineal structures during pregnancy and immediately following obstetric injury. Ultrasound Obstet Gynecol 2008; 32:527–534.
24. Umek WH, Kearney R, Morgan DM. The axial location of structural regions in the urethra: a magnetic resonance study in nulliparous women. Obstet Gynecol 2003;102:1039–1045.
25. Williams AB, Cheetham MJ, Bartram CI et al. Gender differences in the longitudinal pressure profile of the anal canal related to anatomical structure as demonstrated on three-dimensional anal endosonography. Br J Surg 2000;87:1674–1679.
26. Hall RJ, Rogers RG, Saiz L, Qualls C. Translabial ultrasound assessment of the anal sphincter complex: normal measurements of the internal and external anal sphincters at the proximal, mid and distal levels. Int Urogynecol J 2007;18:881–888.
27. Schaefer A, Enck P, Furst G et al. Anatomy of the anal sphincters. Comparison of anal endosonography to magnetic resonance imaging. Dis Colon Rectum 1994;37:777–781.